

Numerical Simulation of Backdraft Phenomena

Andrej Horvat, Yehuda Sinai

Abstract

This paper reports preliminary CFD simulations of backdraft observed in an experimental rig at Lund University. The analysis was performed with the CFX software using the DES turbulence model, a hybrid of LES and RANS, in combination with the EDM combustion model. The DES model uses a RANS formulation in wall proximity to avoid computationally expensive grid resolution that is necessary for realistic LES predictions in wall layers.

The preliminary results are qualitatively promising. The simulations began at the instant at which the door opens. A stream of fresh and cold air enters the enclosure as a gravity current. In the rig, ignition was triggered by flammable conditions existing at a wire, which was constantly heated. In the CFD model the ignition time is computed automatically when flammability conditions are reached inside the enclosure, at the wire, as part of the analysis. Subsequently, the fire front is formed. The deflagration expels fuel-rich mixture into environment, and the combustion continues outside the enclosure as a typical 'secondary' event. Considering that backdraft is a very complex phenomenon, the outcome is considered by the authors to be encouraging.

Nomenclature

Latin letters

C_A, C_B	Eddy-Dissipation model constants
C_{DES}	= 0.61, constant
C_m	= 0.09, constant
D	molecular diffusivity
F_2, F_{DES}	turbulence model blending functions
g	gravity acceleration
h	height of the container
\bar{h}_{tot}	= $c_p \bar{T} + 0.5 \rho \bar{v}_j \bar{v}_j$, total energy
H	Heaviside unit step function
k	turbulence kinetic energy
L	length of the container
p	pressure
Pr	Prandtl number
s	stoichiometric ratio
S	source term, invariant measure of the strain rate
Sc	Schmidt number
t	time
T	temperature
v	velocity
x, y, z	spatial coordinates

Greek letters

β	$\rho_{air} / \rho_{mixture} - 1$
Δ	local grid spacing
ε	turbulence dissipation rate
ϑ	heat of combustion
μ, μ_t	dynamic viscosity, eddy dynamic viscosity
ξ	mass fraction
ρ	density
ψ	molar fraction
ω	turbulence frequency

1 Introduction

One vital aspect of under-ventilated fires is backdraft, which is of particular concern to fire fighters. Descriptions of this phenomenon may be found in any of the textbooks on fire safety, e.g. Drysdale [1], or in a variety of papers and reports [2-7]. Briefly, backdraft is caused by fuel vapour being generated after a fire is extinguished, or reduced in intensity by oxygen starvation, and the subsequent introduction of fresh oxygen, for example by opening of a door. Following the mixing of the fresh air with the fuel-rich environment, concentrations can return to the combustible range, and since ignition sources are likely to exist, flaming combustion may be initiated and can develop into a deflagration.

The current article describes numerical modelling of backdraft using Computational Fluid Dynamics (CFD). The simulations include the initial gravity current that is formed after the door is open, the ignition, spreading of flame in the enclosure, the external fireball, and subsequent decay. The work has simulated one of the experiments conducted at Lund University [7].

Prior to this work, in order to gain insight into the initial stage of backdraft, before ignition, additional numerical simulations of mixing due to the gravity current were performed. For this purpose, use was made of data from the salt water experiments of Fleischmann and McGrattan [8].

Previous work on theoretical modelling of backdraft has ranged from analytical techniques, which are essentially based on lumped-parameter or zonal methodology, to CFD. Examples may be found in the Refs. [3,4,8,9]. In the present work, the numerical simulations start from the instant when the door is opened till the backdraft has decayed inside and outside the compartment. It is also possible to simulate events prior to the door opening, i.e. the under-ventilated fire, but our work has so far focused on the inert mixing and backdraft phenomenon itself. In the Lund experiments [7], the fire which preceded the backdraft was generated by a controlled burner. Regarding situations in which the fire source is uncontrolled, Sinai [10] reported CFD simulation of an under-ventilated fire generated by a liquid (heptane) pool, accounting for coupling between the fire and the fuel, as well as building leakages, and showed that leakages and wall heat transfer can have a major effect on stratification and the fire dynamics. There is also very substantial amount of literature on gravity currents, which have been the subject of extensive study over many years, in many fields, including the environment. Good examples of that work may be found in the books by Turner [11] and Simpson [12]. Recently, Yang et al. [13] reported a successful attempt to simulate an earlier

small-scale backdraft experiment [14], using a laminar flamelet model for partially premixed combustion. Their results gave a comprehensive picture of the phenomenon although without the comparison to the experimental data [14].

The simulations reported here were performed with the CFX-5 commercial CFD code (ver. 5.7). The DES turbulence model and the EDM combustion model were used to model fire spreading through the mixture of methane, air and combustion products. The DES model uses a RANS formulation in wall proximity and the LES model in the bulk of the flow. By switching (automatically) between both models, the required grid resolution and, therefore, computational costs are significantly reduced.

In the Lund experiment, a heated wire was used as the ignition source. An additional ignition model has been developed for the modelling reported here, to initiate the combustion process when conditions at the wire reach the flammable range for methane.

The results have been compared with the experimental data. There is a need for improvement, but considering the complexity of the phenomenon, and uncertainty in the data, the outcome is encouraging.

2 Geometrical considerations and initial assumptions

A CFD model of a full-scale ship container was set up to study fire behaviour during occurrence of backdraft. The modelling is a preliminary exercise aiming to represent one of the experimental tests, although some aspects of the initial conditions had to be estimated because of significant experimental uncertainties in the rig due to leakages [7].

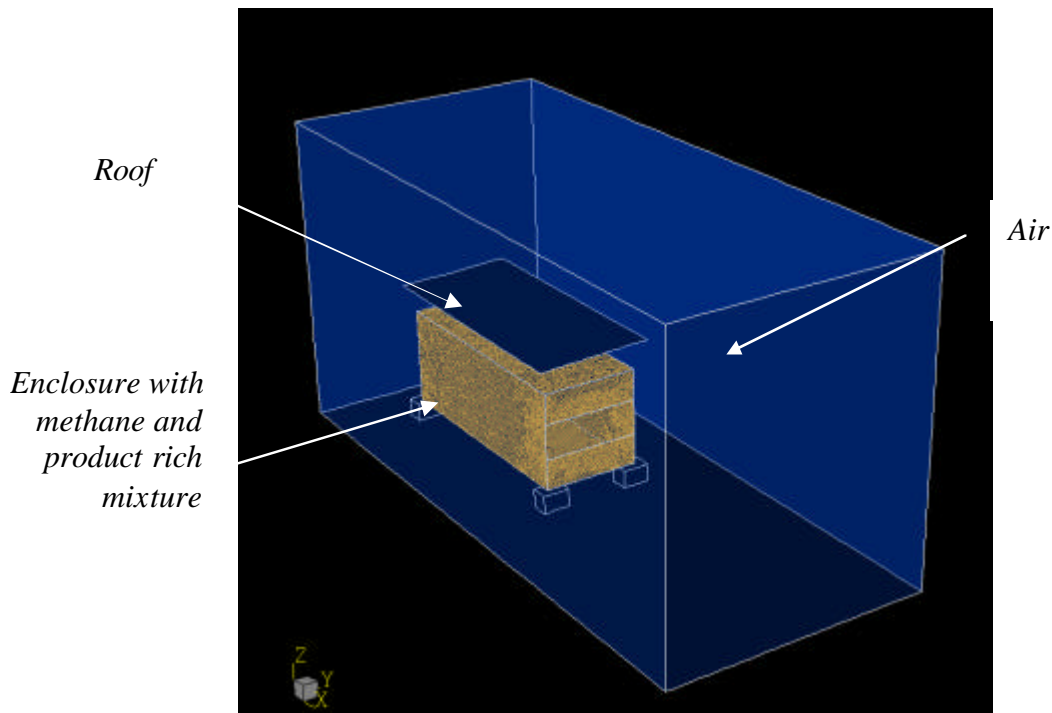


Figure 1: Geometrical arrangement of the backdraft model

The geometry of the model is shown in Fig. 1. The enclosure is 5.5 m long, 2.2 m high and 2.2 m wide. It is positioned in the left half of the simulation domain, which is 14 m long, 7 m deep and 6 m wide. The enclosure is also raised for 40 cm above the ground. A roof plate is positioned nominally 70 cm above the enclosure and is inclined at 5° side to side from the horizontal position. The roof was included in the model because of its potential ability to influence the mixing at the door, as well as external dispersion of the combustible mixture and hence the external fireball. The opening was located in the middle of one end of the enclosure, covering the full width and one third of the container's height.

The numerical simulations were performed from the instant at which the door opens and fresh air enters the compartment. Initially, the container is filled with a mixture that contains methane, air and combustion products. The mixture is rich in unburned methane and combustion products with a relatively small amount of oxygen, which is unable to support burning. Leakages occurred during the tests, and the spatial distribution of the various species

was inhomogeneous but unmeasured. In view of the uncertainties, the following initial composition was assumed in the numerical model:

$$\bar{\Psi}_{\text{CH}_4} = 0.5, \quad \bar{\Psi}_{\text{P}} = 0.25, \quad \bar{\Psi}_{\text{Air}} = 0.25 \quad (\bar{\Psi}_{\text{O}_2} = 0.0525 \text{ and } \bar{\Psi}_{\text{N}_2} = 0.1975). \quad (1)$$

Sensitivity to these initial conditions will be considered and reported later. The initial velocity was set 0.0. Some thermal data were available, and a linear vertical temperature profile was prescribed inside the enclosure:

$$T_{in} = \frac{98^\circ\text{C} - 62^\circ\text{C}}{1.6\text{ m}}(z + 0.7\text{ m}) + 62^\circ\text{C} \quad , \quad (2)$$

as measured in the experimental case No.9 after 420 s [7]. For the external initial composition we assumed fresh air:

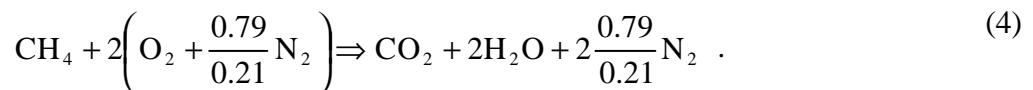
$$\bar{\Psi}_{\text{CH}_4} = 0.0, \quad \bar{\Psi}_{\text{P}} = 0.0, \quad \bar{\Psi}_{\text{Air}} = 1.0 \quad (\bar{\Psi}_{\text{O}_2} = 0.21 \text{ and } \bar{\Psi}_{\text{N}_2} = 0.79), \quad (3)$$

and an initial temperature of 5 °C.

For simulations' boundary conditions, the no-slip, smooth, adiabatic boundary conditions were set for all walls. At the outermost boundaries of the domain, wall conditions were set at the floor and pressure conditions ('openings') at the remaining boundaries, with an ambient temperature of 5 °C. At openings, flow may enter or leave, depending on the local pressure just inside the boundary.

3 Modelling approach

In the numerical experiment the following single step chemical reaction was used to model conversion of chemical species:



The methane (CH₄) reacts with oxygen (O₂) producing carbon dioxide (CO₂) and water (H₂O). The nitrogen (N₂) is a diluent.

Due to the turbulent flow regime, the fluid flow transport equations have to be written in their (Favré) averaged form [15]. The mass transport equation for the mixture:

$$\partial_t \rho + \partial_j (\rho \bar{v}_j) = 0 \quad , \quad (5)$$

has to be solved together with the transport equation for the components CH₄, O₂, H₂O and CO₂:

$$\partial_t (\rho \bar{\xi}_c) + \partial_j (\rho \bar{v}_j \bar{\xi}_c) = \partial_j (\rho D_c \partial_j \bar{\xi}_c) + \bar{S}_c - \partial_j (\rho \overline{v_j' \xi_c'}) \quad , \quad (6)$$

where $\bar{\xi}_c$ is a mass fraction of the component c and S_c is a source term due to the chemical reaction involving component c .

The momentum transport equation was used in its compressible form:

$$\partial_t (\rho \bar{v}_i) + \partial_j (\rho \bar{v}_j \bar{v}_i) = -\partial_i \bar{p} + \partial_j \left(\mu (\partial_j \bar{v}_i + \partial_i \bar{v}_j) - \frac{2}{3} \mu (\partial_l \bar{v}_l) \delta_{ji} \right) + g(\rho - \rho_{ref}) - \partial_j (\rho \overline{v_j' v_i'}) \quad (7)$$

Furthermore, the energy equation has to be written for the total specific enthalpy:

$$\partial_t (\rho \bar{h}_{tot}) - \partial_t p + \partial_j (\rho \bar{v}_j \bar{h}_{tot}) = \partial_j (\lambda \partial_j \bar{T}) + \sum_n \vartheta_n \bar{S}_c - \partial_j (\rho \overline{v_j' h_{tot}'}) \quad (8)$$

3.1 Turbulence modelling

In the present work, a Detached Eddy Simulation (DES) model was used to model turbulence. The DES model was proposed by Strelets [16] and later extended by Menter and Kuntz [17]. It is an attempt to combine elements of RANS and LES formulations in order to arrive at a hybrid formulation. Namely, using the Large Eddy Simulation (LES) turbulence model to resolve flow structures in wall boundary layer flows at high Re numbers is extremely

expensive computationally and, therefore, not useful for most industrial flow simulations (unless wall effects are insignificant). To reduce computational costs, the DES model applies the Shear Stress Transport (SST) model inside attached and mildly separated boundary layers, and the LES model in massively separated regions, where turbulence length scale is much larger. In this way, the DES model preserves accuracy of the SST model to approximate the boundary layer and the ability of the LES model to resolve time dependent flow structures despite relatively modest grid size. The Menter & Kunz formulation is reproduced below.

In the DES model, a turbulence length scale calculated as

$$l_{RANS} = \frac{\sqrt{k}}{C_\mu \omega}, \quad (9)$$

is compared with a length scale associated with the local grid spacing Δ and the LES model:

$$l_{LES} = C_{DES} \Delta. \quad (10)$$

The DES model switches from the SST model to the LES model in the regions where the turbulence length scale l_{RANS} is larger than the local LES model scale l_{LES} .

The turbulence kinetic energy is calculated as

$$\partial_i(\rho k) + \partial_j(\rho \bar{v}_j k) = \partial_j \left(\left(\mu + \frac{\mu_t}{\sigma_{k3}} \right) \partial_j k \right) + \tilde{P} - F_{DES} C_\mu \rho \omega k, \quad (11)$$

where \tilde{P} is turbulence production due to shear stresses and buoyancy. F_{DES} is a blending function,

$$F_{DES} = \max \left(\frac{l_{RANS}}{l_{LES}} (1 - F_2), 1 \right), \quad (12)$$

which switches between the RANS and the LES model scale. The blending function F_2 used in the expression reduces the sensitivity to a local mesh arrangement.

Turbulence eddy frequency ω is calculated with the following transport equation:

$$\partial_t(\rho\omega) + \partial_j(\rho\bar{v}_j\omega) = \alpha_3\rho S^2 + \partial_j\left(\left(\mu + \frac{\mu_t}{\sigma_{\omega 3}}\right)\partial_j\omega\right) + (1 - F_1)\frac{2\rho}{\sigma_{\omega 2}}\partial_j k \partial_j\omega - \beta_3\rho\omega^2 \quad (13)$$

Turbulent viscosity is defined as in the SST model:

$$\mu_t = \frac{a_1 k}{\max(a_1\omega, F_2 S)} \quad (14)$$

where S is an invariant measure of the strain rate.

The turbulence heat fluxes are defined as

$$\overline{\rho v_j' h_{tot}'} = -\frac{\mu_t}{Pr_t} \partial_j \bar{h}, \quad (15)$$

where the turbulent Prandtl number Pr_t is empirically determined. As usual, the turbulence mass fluxes are calculated as

$$\overline{\rho v_j' \xi'} = -\frac{\mu_t}{Sc_t} \partial_j \bar{\xi}, \quad (16)$$

where Sc_t is the turbulent Schmidt number. Usually the molecular mass diffusivity ρD is small compare to the turbulence mass diffusivity μ_t/Sc_t and often unknown.

Note that the parameters σ_{k3} , α_3 , $\sigma_{\omega 3}$, β_3 and F_2 are not constants. Their values are calculated locally during the simulations. More details on calculation of the DES model parameters can be found in the Refs. [17,18].

3.2. Combustion modelling

For the backdraft simulations, we selected an eddy-dissipation combustion model, which is based on the concept that the chemical reaction is fast relative to the transport processes in the flow. When reactants mix at the molecular level, they instantaneously form products. This means that the Damköhler number is large. The model assumes that the reaction rate may be

related directly to the time required to mix reactants at the molecular level. Therefore, the level of turbulent mixing is a controlling condition for successful combustion reaction. Reaction kinetics are not taken into account in this model.

The eddy dissipation model is based on the Eddy-Break-Up (EBU) model that was originally proposed by Spalding [19]. In his model, the combustion reactions are lumped together in a one step reaction. For turbulent flow, the reaction rate depends on the flow timescale $t_{flow} = k/\varepsilon$, which is a time needed for an eddy to dissipate, and the variance of fuel in the flow. Magnussen and Hjertager [20] developed the concept further. In their eddy-dissipation model, the mass fractions of fuel, oxidizer and products determine the reaction rate. Consequently, the source term in the transport equation (6) for the fuel mass fraction is

$$S_{f,EDM} = -\rho C_A \frac{\varepsilon}{k} \min \left(\bar{\xi}_f, \frac{\bar{\xi}_{Ox}}{s}, C_B \frac{\bar{\xi}_p}{1+s} \right) \quad (17)$$

where s is stoichiometric ratio, and C_A and C_B are empirical constants.

The constant C_A was set to 8.0 in the backdraft simulations. Due to the product-rich environment, the product dependence of the reaction rate was dropped from (17). The source term $S_{f,EDM}$ was multiplied by $H(T-T_{ext})$, where H is the Heaviside unit step function, which is zero when its argument is negative, and 1 when it is positive. T_{ext} is a global extinction parameter, which cannot be identified with the local extinction or auto-ignition temperature since it must also account for turbulent fluctuations of temperature, flame stretch as well as local extinction and re-ignition effects. It is therefore treated as an adjustable modelling parameter. Some experimentation with its influence was carried out, and a value of 600K has been adopted. High values of T_{ext} led to failure of the flame to propagate, and low values led to excessive pressures.

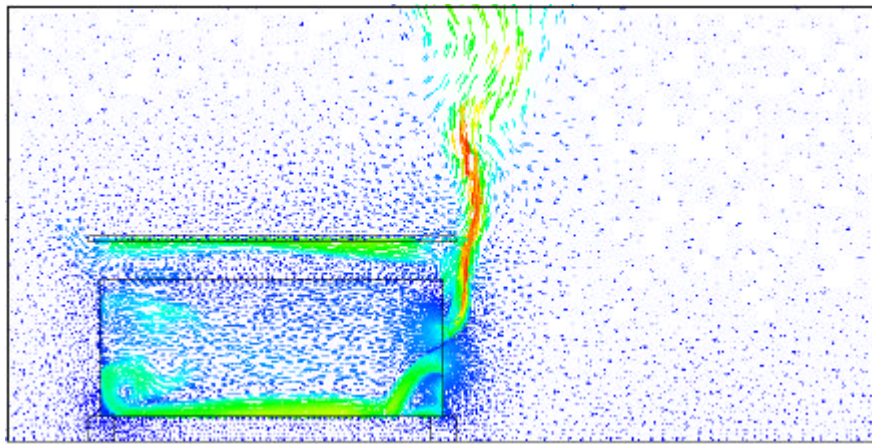
4 Simulation results and discussion

Three-dimensional numerical mesh with 431418 grid nodes was generated to perform the analysis. The mesh consisted of tetrahedra and prisms; the latter are aligned with walls to improve resolution of the boundary layer structure. The average mesh spacing inside the enclosure was 10 cm. In addition, the mesh was further refined around the container entrance. As numerical results can be grid dependent, special care was taken to construct numerical grids with sufficient resolution and uniformity.

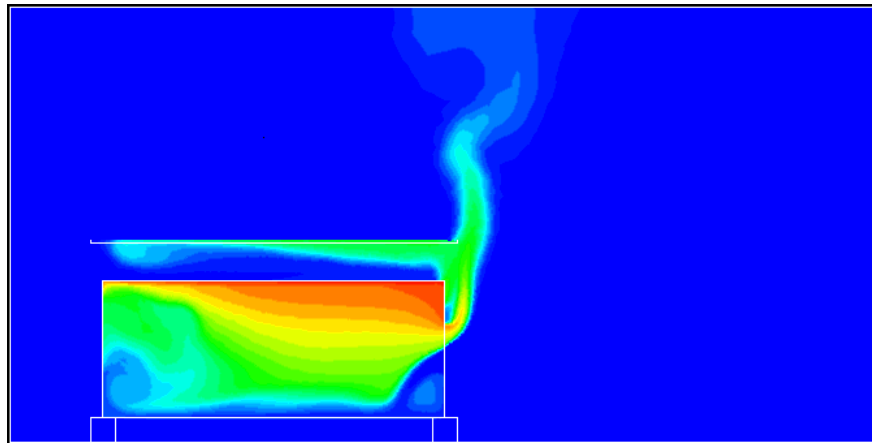
The initial timestep was set to $\Delta t = 0.015$ s taking into account the timescale $L/\sqrt{\beta gh}$ of the initial gravity wave behaviour. In the experiments the ignition was achieved with a hot wire [7]. In the numerical model, methane and oxygen concentrations were checked in a small cylindrical volume at the back of the enclosure, 15 cm from the wall, at each timestep. If the methane concentration was locally within its flammability range ($0.05 < \bar{\Psi}_{CH_4} < 0.15$) [1], a thermal energy source was imposed temporarily. A more refined assessment of the flammability range, accounting for the varying concentrations of diluents, has also been tested and was not found to yield significant differences. After ignition was reached, the time step was reduced to $\Delta t = 0.0005$ s and then slowly increased to $\Delta t = 0.002$ s .

From the simulation results, instantaneous fields of velocity, pressure, temperature and mass fractions were obtained. Figures 2 show the instantaneous fields before the ignition ($t = 7.2$ s), during occurrence of a gravity wave. The stream of fresh and cold air enters the enclosure and moves along the bottom toward the back wall. It can be identified as a high velocity region (Fig. 2a) with low temperature (Fig. 2b) and low mass fraction of methane (Fig. 2c). As it

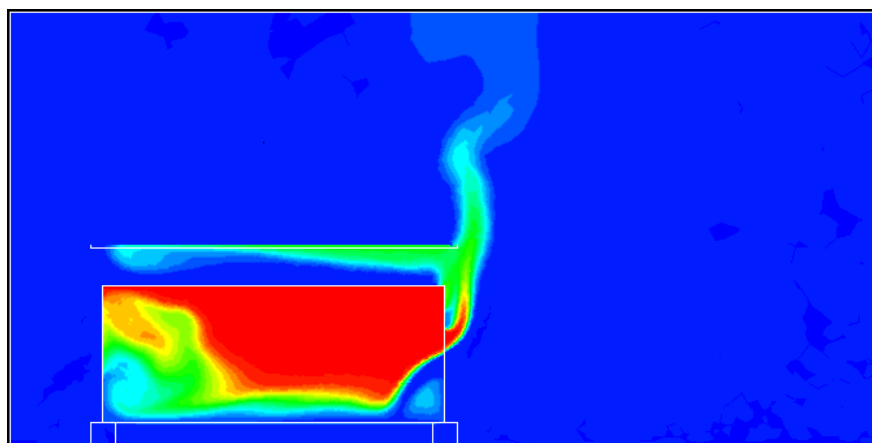
reflects from the back wall, a large premixed region is created, where the mixture is within the flammability limits [1].



$0 \text{ m/s} < v < 3.5 \text{ m/s}$ (a)



$280 \text{ K} < T < 380 \text{ K}$ (b)



$0.0 < \bar{\xi}_{\text{CH}_4} < 0.36$ (c)

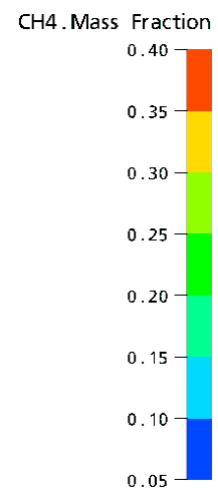
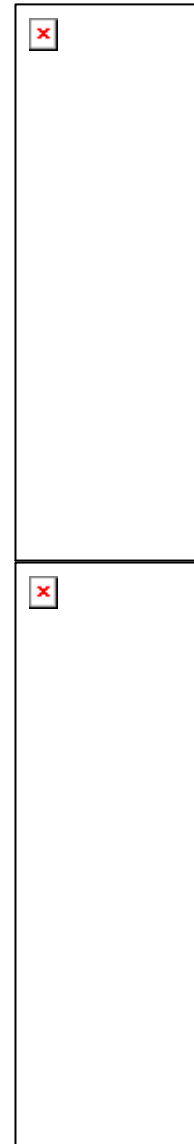


Figure 2: The instantaneous fields during the occurrence of a gravity wave at $t = 7.2 \text{ s}$.
 (a) velocity, (b) temperature and (c) methane mass fraction

The ignition point was reached at $t_{ign} = 11.4$ s. The time of ignition was compared with the experimental data [7] and presented in Table 1.

Table 1: Comparison of the time to ignition; the experimental data for mixed methane concentration are calculated from supply vessel weight measurements [7]

	$\bar{\Psi}_{CH_4}$	t_{ign} [s]
Gojkovic [7], exp. no. 4	0.35	35
Gojkovic [7], exp. no. 7	0.28	46
Gojkovic [7], exp. no. 9	0.31	25
Gojkovic [7], exp. no. 10	0.27	15
Gojkovic [7], exp. no. 11	0.20	32
Gojkovic [7], exp. no. 12	0.27	34
Gojkovic [7], exp. no. 13	0.23	22
Numerical simulation	0.50	11.4

The calculated ignition time is smaller than the ignition time observed in the experiments [7]. The difference may partly be due to different identification of the ignition event. In the experiments, the ignition time is determined by visual identification of fire, whereas in the numerical calculation, the ignition time marks reaching the flammability limits around the ignition point device, thus triggering the ignition algorithm. Note that the ignition time in the tests was observed to be non-repeatable, and indeed in some nominally identical tests, backdraft did not occur at all.

Figures 3 show the instantaneous fields of velocity, temperature and mass fraction of methane after the ignition at $t = 11.6$ s.

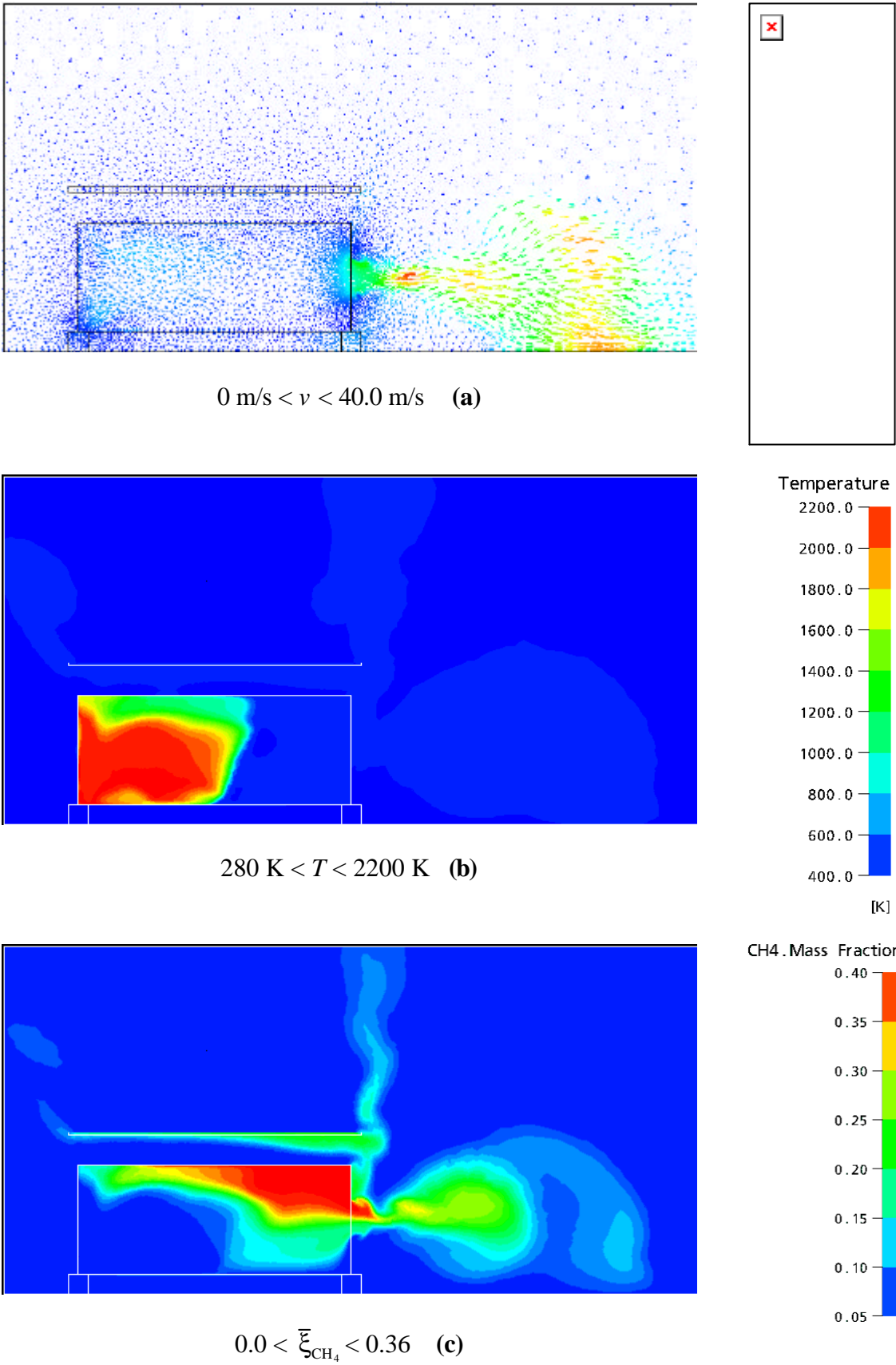


Figure 3: The instantaneous fields after the ignition at $t = 11.6$ s.
 (a) velocity, (b) temperature and (c) methane mass fraction

At this stage, the flame front has propagated over half of the container (Fig. 3b). The expanding products of combustion accelerate the flow from the container to the external environment. The local velocity of gases around the opening increases up to 40 m/s (Fig. 3a). Mass fractions of methane and oxygen rapidly decrease in the area of the fire; some of the fuel is also pushed out of the enclosure (Figs. 3c).

Figures 4 show the instantaneous fields of velocity, temperature and mass fraction of methane when the fire front has propagated outside the enclosure ($t = 11.6$ s). When the fire front reaches the door, combustion continues outside the enclosure as the fuel has been pushed through the door (Fig. 4b). Eventually, as the fuel mass fraction decreases (Fig. 4c), the temperature inside the enclosure also decreases.

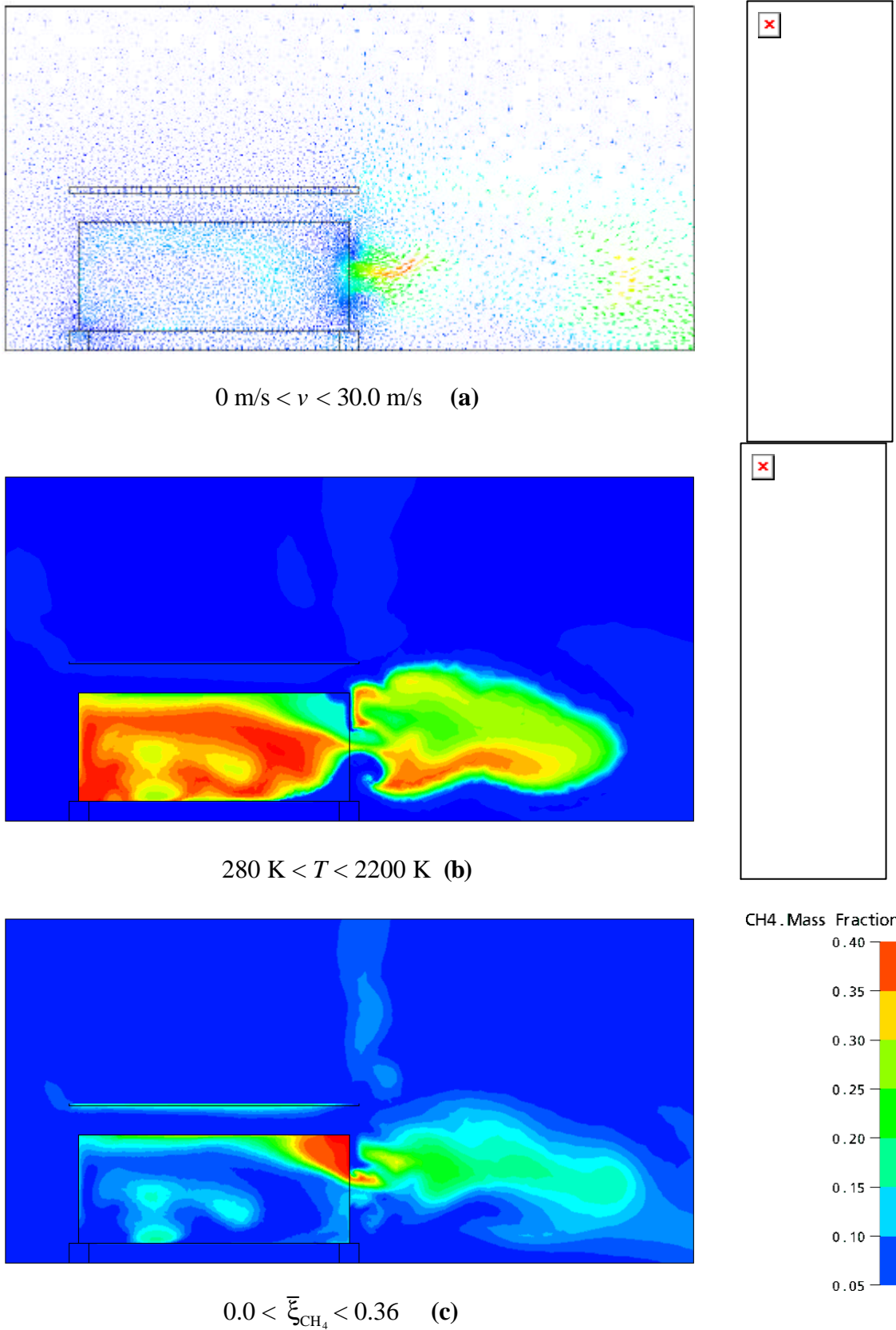


Figure 4: The instantaneous fields during backdraft at $t = 12.0$ s.
 (a) velocity, (b) temperature and (c) methane mass fraction

Time distributions of relative pressure ($p-p_{amb}$) and temperature after the ignition were also compared with the measured values [7]. Unfortunately, the time interval between temperature measurements is too long for reliable comparison of results. Nevertheless, some conclusions can be obtained from the currently available sets of data.

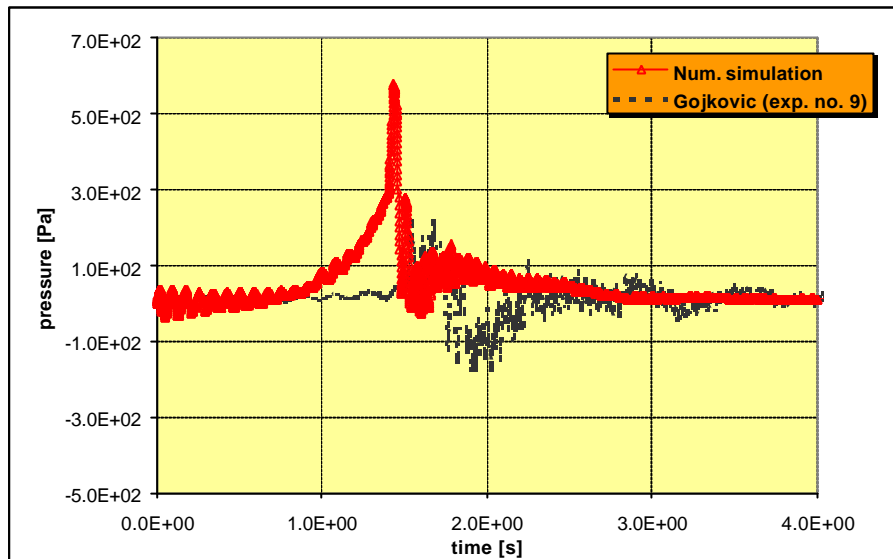


Figure 5: Time distribution of relative pressure after ignition

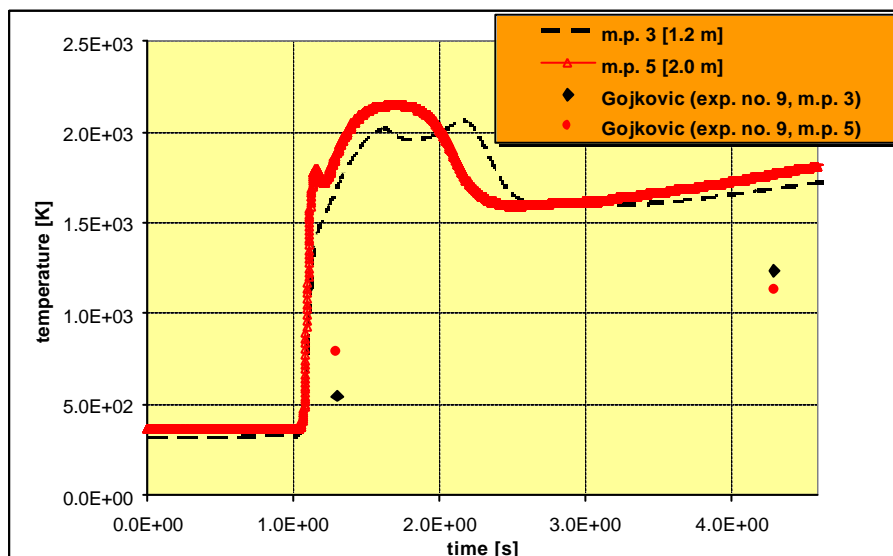


Figure 6: Time distribution of temperature after ignition

Figure 5 shows comparison between the calculated time distribution of relative pressure and a record taken from the pressure sensor in the experimental rig. The present combustion model is simple and computationally very efficient. Unfortunately, it only barely takes into account the reaction kinetics, which depends on local and temporal chemical composition and temperature. As a consequence, the total amount of consumed fuel is larger than seen in the experiments. This leads to a slightly faster flame front, which produces stronger pressure pulse (Fig. 5) and higher temperatures (Fig. 6).

5 Conclusions

Numerical simulations of one of the backdraft experiments performed at Lund University were conducted. The simulations considered the system from the time at which the enclosure was opened. Thus, the inert gravity current which precedes the backdraft was computed as part of the simulation. The DES turbulence model and EDM combustion model were used to model turbulence behaviour and combustion. The ignition model, which has been developed for this project, initiated the combustion process when conditions at any part of the heated wire in the rig reached concentrations which lay within the flammable range.

The model predicted ignition after about 12 seconds, and a propagating flame, which generated speeds of tens (up to about 40) of metres per second at or near the door. The analysis indicated that burning occurred not only inside the compartment, but also outside, caused by the expulsion of fuel gas from the compartment upstream of the primary flame front. The predicted ignition time agrees qualitatively with the experimental data, whilst no data is available for the flow speeds. Differences between the simulations and the data are greater for pressure and temperature. This is probably attributable to possible shortcomings in the ignition and combustion models, inaccuracies in the gravity current prediction, and

perhaps slow frequency response of the instrumentation [7]. Whilst errors in the predicted ignition time are not vital in the practical sense, they may be symptomatic of inadequacies of the modelling. It should be noted that Gojkovic reported that the experiments were not always repeatable, and in some nominally identical situations, backdraft was observed in one test but not another. Bearing in mind that backdraft is a very complex phenomenon, the outcome is considered by the authors to be encouraging. Nevertheless, the work is continuing, with the aim of improving the quality of the predictions.

Acknowledgments

The authors have pleasure in acknowledging the assistance of Daniel Gojkovic and Bjorn Karlsson in providing and clarifying data from the Lund rig. The present work was performed as a part of the project "Under-Ventilated Compartments Fires (FIRENET)" (Co. No. HPRN-CT-2002-00197). The project is supported by the EU Research Training Network FP5, which is gratefully acknowledged.

References

1. Drysdale, D., "An Introduction to Fire Dynamics", John Wiley & Sons, 1990.
2. Dunn, V., "Beating the Backdraft", Fire Eng., Vol. 14, pp. 44-48, 1988.
3. Fleischmann C.M., "Backdraft Phenomena", NIST-GCR-94-646, NIST, Gaithersburg, MD, 1994.
4. Bukowski, R.W., "Modelling backdraft: The fire at 62 Watts Street", NFPA J., Vol. 89, pp. 85-89, 1995.
5. Gottuk D.T., Peatross M.J., Farley J.P. & Williams F.W., "The development and mitigation of backdraft: A real-scale shipboard study", Fire Safety Journal, Vol. 33, pp.

- 261-282, 1999.
6. Foster J.A. & Roberts G.V., "An Experimental Investigation of Backdraft", Fire Research Division, ODPM, London, December 2003.
 7. Gojkovic, D., "Initial Backdraft Experiments", Report 3121, 2000, Department of Fire Safety Engineering, Lund University, Sweden.
 8. Fleischmann, C.M., McGrattan, K.B., "Numerical and Experimental Gravity Currents Related to Backdrafts", Fire Safety Journal, 1999, Vol. 33, pp. 21-34.
 9. Weng W.G. & Fan W.C., "Nonlinear analysis of the backdraft phenomenon in room fires", Fire Safety Journal, Vol. 39, pp. 447-464, 2004.
 10. Sinai Y.L., "Comments on the Role of Leakages in Field Modelling of Under-Ventilated Compartment Fires", Fire Safety Journal, Vol. 33, pp. 11-20, 1999.
 11. Turner J.S., "Buoyancy Effect in Fluids", Cambridge University Press, 1973.
 12. Simpson J.E., "Gravity Currents in the Environment and the Laboratory", Wiley, New York, 1987.
 13. Yang, R., Weng, W.G., Fan, W.C., Wang, Y.S., "Subgrid Scale Laminar Flamelet Model for Partially Premixed Combustion and Its Application to Backdraft Simulation", Fire Safety Journal, Vol. 40, 2, 2005, pp. 81-98.
 14. Weng, W.G., Fan, W.C., Yang, L.Z., Song, H., Deng, Z.H., Qin, J., Liao, G.X., "Experimental Study of Backdraft in a Compartment with Openings of Different Geometries", Combustion and Flame, 132, 2003, pp. 709-714.
 15. CFX Online Documentation, <http://www-waterloo.ansys.com/cfxcommunity/technotes/documentation/>.
 16. Strelets, M., "Detached Eddy Simulation of Massively Separated Flows", AIAA 2001-0879, 2001.
 17. Menter, F. R., Kuntz, M., "Development and Application of a Zonal DES Turbulence Model for CFX-5", CFX-Validation Report, CFX-VAL17/0503.

18. Horvat, A., Sinai, Y.L., “Progress Report for the Period 1 June 2003 – 31 May 2004”, ANSYS/CONS/892/R1, Firenet - EU Training Network, June, 2004.
19. Spalding, D.B., “Mixing and Chemical Reaction in Steady Confined Turbulent Flames”, The 13th Symp. (Int.) on Combustion, 1971, Proceedings, pp. 649-657.
20. Magnussen, B. F. and Hjertager, B. H., “On Mathematical Modeling of Turbulent Combustion with Special Emphasis on Soot Formation and Combustion”, The 16th Symp. (Int.) on Combustion, 1976, Proceedings, pp. 719–729.